RESEARCH ARTICLE | OCTOBER 12 2020

Stretchable bioelectronics: Mitigating the challenges of the percolation threshold in conductive elastomers

Special Collection: Advances in Bioelectronics: Materials, Devices, and Translational Applications

Alexey Novikov; Josef Goding; Christopher Chapman; ... et. al

APL Mater 8, 101105 (2020)
https://doi.org/10.1063/5.0005410

Stretchable bioelectronics: Mitigating the challenges of the percolation threshold in conductive elastomers

Cite as: APL Mater. 8, 101105 (2020); doi: 10.1063/5.0005410
Submitted: 24 February 2020 • Accepted: 8 September 2020 •
Published Online: 12 October 2020

Alexey Novikov,[1,2] Josef Goding,[1] Christopher Chapman,[1] Estelle Cuttaz,[1] and Rylie A. Green[1,a)]

AFFILIATIONS

[1] Department of Bioengineering, Imperial College London, London SW7 2BP, United Kingdom
[2] Department of Physics, Centre for Processable Electronics, Imperial College London, London SW7 2AZ, United Kingdom

Note: This paper is part of the Special Topic on Advances in Bioelectronics.
[a)] **Author to whom correspondence should be addressed:** rylie.green@imperial.ac.uk

ABSTRACT

Conductive polymer (CP)–elastomer composites have been proposed as an alternative to the metals conventionally used for bioelectronic devices. Being softer and more stretchable than metals such as platinum and gold, they can mitigate the adverse effects associated with mechanical mismatch and fatigue failure. Such composites are conventionally made by embedding CP particles inside an elastomeric matrix. However, to achieve such a structure, a high CP loading that reaches a percolation threshold is required. High percolation thresholds lead to the degradation of mechanical properties. This study presents an alternate approach designed to reduce the CP content while maintaining conductivity through the matrix. A poly(3,4-ethylenedioxythiophene)-polystyrene sulfonate (PEDOT:PSS) composite was produced by filling a CP aerogel with polydimethylsiloxane (PDMS). This approach successfully formed a stretchable, conductive material, with only 1.8 wt. % CP. While elastic behavior was observed at low strain, the composite displayed plastic deformation at high strain (>20%). Future improvements will focus on the modification of the PEDOT:PSS–PDMS interface, to improve interaction of the polymer components and, hence, mechanical stability within the construct.

INTRODUCTION

Bioelectronics comprise a group of devices used for stimulation and recording of electrically excitable tissues. These medical devices have a wide range of applications and have proven to be especially useful in invasive neural and cardiac interventions (Normann, 2007; Shepherd *et al.*, 2013; and Timperley *et al.*, 2007). Metals and metallic alloys, being widely used in electrical engineering, have been the most popular choice of materials both to conduct charge within leads and to inject charge at the tissue–electrode interface (Cogan, 2008; Green *et al.*, 2013; and Haqqani *et al.*, 2018). However, metallic bioelectronics possess a range of disadvantages. Metals have a much higher stiffness than living tissue, with an elastic modulus of over 100 GPa compared to soft tissue at 0.5 kPa–500 kPa (Feig *et al.*, 2018; Fung, 2013; Landers *et al.*, 2002; and Polikov *et al.*, 2005). This strain mismatch leads to cell death and fibrosis of the tissue–device interface, resulting in a loss of signal transduction (Huang and Baba, 1972; Lo, 1998; Moore and Shannon, 2009; and Polikov *et al.*, 2005). This process can significantly impact device safety and efficacy, subjecting recipients to further health risks. Additionally, relatively low charge injection limits (CIL) of metallic electrodes also inhibit bioelectronic device performance, by limiting the amount of electrochemical charge which can be transported to the excitable tissue without the occurrence of unwanted, irreversible chemical reactions at the device–tissue interface (Cogan *et al.*, 2005; Cuttaz *et al.*, 2019; Merrill *et al.*, 2005; and Tandon *et al.*, 2009). Metallic components also have poor compatibility with magnetic fields used during magnetic resonance imaging (MRI), which is particularly problematic for cardiac pacemaker recipients (Ferreira *et al.*, 2014; Kalin and Stanton, 2005; Levine *et al.*, 2007; and Nordbeck *et al.*, 2015). MRI-induced heat and current pose a serious threat to patient health and prohibit

clinicians from using the full range of MRI diagnostics and monitoring. This limits the capacity to identify problems with pacing leads interacting with cardiac tissues (Ferreira *et al.*, 2014; Nordbeck *et al.*, 2015).

Conductive polymer (CPs) present an alternative material platform that mitigates the drawbacks of metallic materials. CPs are considerably less stiff than metals, with an elastic modulus in the MPa range (Baek *et al.*, 2014; Feig *et al.*, 2018; Hassarati *et al.*, 2014; Rivnay *et al.*, 2017; 2014; and Tahk *et al.*, 2009). CPs such as polypyrrole (PPy), polyaniline (PANI), and poly(3,4-ethylenedioxythio phene) (PEDOT) have been shown to shield electromagnetic hazards (Kim *et al.*, 2011; Li *et al.*, 2016; and Wang and Jing, 2005), alleviating the limitations on patient diagnostics. PEDOT, in particular, has shown promising charge injection capabilities, increasing the capacity to modulate cardiac and neural tissues at therapeutic levels with lower voltage and, hence, safer operational parameters for patients (Cogan, 2008; Cuttaz *et al.*, 2019). Nonetheless, pure CPs lack mechanical robustness, and in most cases, CP products are constrained to films and coatings due to their friability (Baek *et al.*, 2014; Hassarati *et al.*, 2014; and Wang *et al.*, 2017). Though much softer than metals and alloys, pure CPs still have limited conformability with biological tissue (Feig *et al.*, 2018). Therefore, a substantial effort is being made in the field of soft bioelectronics to enhance the mechanical properties of the CPs and develop a well-performing conductive polymer hybrid (Feig *et al.*, 2018; Kaur *et al.*, 2015; Patton *et al.*, 2016; Wang *et al.*, 2017; and Yuxin *et al.*, 2018).

One of the most popular strategies has been to develop composites or hybrids of CPs, where the CP is integrated with a more mechanically stable polymer. This has led the development of conductive hydrogels (CHs) and conductive elastomers (CEs) (Cuttaz *et al.*, 2019; Feig *et al.*, 2018; Kaur *et al.*, 2015; Patton *et al.*, 2016; and Yuxin *et al.*, 2018). These composites can be formed by either growing CP chains within the secondary polymer, synthesizing copolymers of short CP chains bonded to a non-conductive polymer, laminating a CP film on top of a more stable polymer substrate, or dispersing CPs within a pre-polymer matrix (Cuttaz *et al.*, 2019; Da Silva *et al.*, 2018; Kaur *et al.*, 2015; Patton *et al.*, 2016; and Yuxin *et al.*, 2018).

Each of these methods are challenging and present different trade-offs between the mechanical and electrical properties of the final material [Fig. 1, (Patton *et al.*, 2015)]. While CPs can be easily grown within a hydrogel matrix, the resulting CH material is not feasible as a standalone material for bioelectronics, being water and ion permeable and experiencing high volumetric swelling in a biological environment (Goding *et al.*, 2019; Patton *et al.*, 2015). Elastomeric materials present high steric hindrance to the growth of CPs once the elastomer is cured, and this results in a material with negligible conductivity. Chemical strategies to create copolymers do not produce materials with significant electrical properties, as the continuous conjugated backbone required to impart electrical conduction within the CP component is sterically hindered by the segments of non-conductive polymer backbone (Da Silva *et al.*, 2018; Luebben *et al.*, 2004; and Yagci and Toppare, 2003). Layered composites present high conductivity in undeformed forms, as the CP component is formed in a continuous sheet. However, these composite structures suffer from strain mismatch between the CP and the underlying substrate. This mismatch causes cracks and other defects such as buckling in the CP layer upon repeat stretching, eventually resulting in delamination and conductivity loss (Patton *et al.*, 2016; Sasaki *et al.*, 2014; and Sekine *et al.*, 2010). Composites made from dispersions are commonly fabricated by blending CP chains within the pre-polymer solution of a hydrogel or elastomer (Cuttaz *et al.*, 2019; Kaur *et al.*, 2015; and Patton *et al.*, 2016). They can also be formed by *in situ* polymerization of the CP within the secondary polymer matrix (Kaur *et al.*, 2015; Patton *et al.*, 2016). However, to exhibit high conductivities, these composites need to reach a percolation threshold, reflecting a CP concentration where the conductive component is present in high enough amounts to form interpenetrating networks throughout the bulk polymer (Kaur *et al.*, 2015; Patton *et al.*, 2016). For most composites and, in particular, for CEs, reaching the percolation threshold results in the degradation of the mechanical properties of the hybrid due to high concentrations of brittle CP within the network (Cuttaz *et al.*, 2019; Patton *et al.*, 2016). It is clear that while CP based electronics have significant benefits over their metallic counterparts, there is a need to improve the way in which CP composites are fabricated. The critical challenge is in improving the CP integration with the mechanically supporting polymer such that the resulting composite has high conductivity while preserving the flexibility.

Recently, Feig *et al.* (2018) presented an alternative approach to fabricating conductive hydrogel composites. In contrast to the conventional methods, which add the CP to a hydrogel matrix, this approach suggested that a supporting polymer matrix can be *in situ* polymerized within a preformed CP template (Feig *et al.*, 2018). This was achieved by soaking a poly(3,4-ethylenedioxythiophene)-polystyrene sulfonate (PEDOT:PSS) hydrogel in polymer precursors and, subsequently, using thermal polymerization to form a supporting secondary polymer network (Feig *et al.*, 2018). The most valuable advantage of this strategy was that connected and, hence, conductive CP networks were created during initial formation of PEDOT:PSS, which mitigates the need for a percolation threshold. However, in the study by Feig *et al.* (2018), the secondary polymer matrix was a flexible polyacrylic acid hydrogel, and although hydrogels are soft and compliant with human tissues, many variants are non-elastic, and being hydrophilic enables fluid ingress and electrical cross talk within device components. As such, conductive hydrogel composites have limited potential as standalone materials in clinical bioelectronic applications and cannot be used to replace conduction pathways in cardiac pacemaker leads or bionic device electrode arrays (Dai *et al.*, 2010; 2009; Feig *et al.*, 2018; and Patton *et al.*, 2016).

Taking inspiration from the templated hydrogel CP composite, this study explored the capacity to produce CE composites by first forming the CP network and, subsequently, introducing the elastomer support. It was hypothesized that functional conductive materials could be achieved by curing an elastomer matrix within an open preformed CP network and that such a structure would enable use of lower CP concentrations compared to conventional CEs, mitigating the need to reach a percolation threshold and, thereby, preserving the mechanical properties of the composite. This research aimed to develop and study a CE composite based on continuous PEDOT networks filled with polydimethylsiloxane (PDMS). The PEDOT:PSS hydrogels were prepared as described by Yao *et al.* (2017) and lyophilized to create an open pore aerogel. This CP aerogel network was then filled with the PDMS elastomer, and the composite was cured to remove solvents. The PEDOT:PSS–PDMS

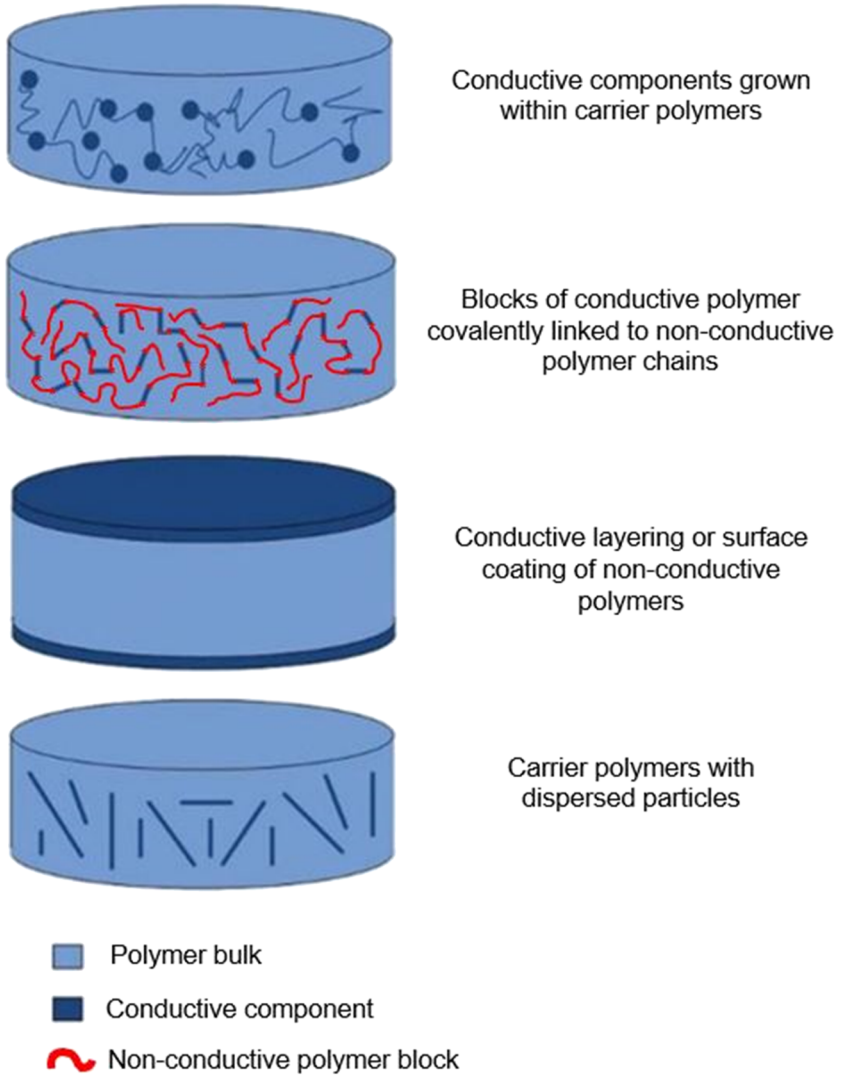

FIG. 1. Types of CEs. Adapted from Patton *et al.* (2015).

composite was characterized for chemical structure, functional electrical properties, and dynamic mechanical performance. The conductivity enhancement resulting from this method was assessed by comparison with the conventional approaches previously reported in the literature.

EXPERIMENTAL METHODS

Material preparation

For hydrogel preparation, an aqueous dispersion of PEDOT:PSS (PH1000, M122 Ossila Ltd.) and concentrated sulfuric acid (99.999%, 339741 Sigma-Aldrich) was used. The sulfuric acid was chosen as a low cost and readily accessible gelling agent. The two components were mixed for 5 min to obtain a PEDOT:PSS/acid mixture with an acid concentration of 0.1M. The mixture was placed in a 90 °C oven for 3 h to undergo gelation. The resultant hydrogels were purified by washing 3× with deionized (DI) water to ensure removal of excess PSS and acid. The hydrogels were then freeze-dried to obtain aerogels.

CE composites were produced by filling the aerogels with 40 wt. % PDMS in a hexane solution. Sylgard 184 (a two part PDMS and curing agent) was mixed at a 10:1 volume ratio prior to dilution with hexane (24 580 VWR). The resultant solution was then poured into glass vials with the aerogels. To promote full penetration of the PDMS solution, samples were exposed to vacuum cycling between 300 mbar and atmospheric pressure (1 h cycle period) for 24 h. Samples were left at RT for one week to allow the PDMS to cure and the hexane to evaporate.

Physical characterization

Aerogel and composite cross sections were imaged using optical and scanning electron microscopy (SEM, JSEM 6010LA). In

addition, energy dispersive x-ray (EDX) spectroscopy was conducted to obtain PEDOT:PSS and PDMS distribution maps. For this study, sulfur acted as a reference element for PEDOT:PSS, while silicon represented PDMS.

The optical profilometer was used to acquire a topographical map of the CE composite surface (Olympus Laser Scanning Microscope LEXT OLS5000). Color code mapping was used to determine features of the surface. In addition, arithmetical mean heights were computed for areas of interest.

Mechanical characterization

Mechanical characterization was conducted on the PEDOT:PSS hydrogels, lyophilized PEDOT:PSS aerogels, pure PDMS, and CE composites. 24 well-plates were used as molds for the hydrogel preparation. Purified hydrogels were prepared in the form of cylinders, with 10 mm thickness and 15 mm in diameter. Following lyophilization, the aerogel samples were found to be 5 mm in thickness with a 10 mm diameter. The PDMS and CE composite samples were also of a cylindrical shape, but a punch tool was used to make samples of 5 mm in thickness and 4 mm in diameter. Prior to the punching, a razor blade and abrasive paper were used to smooth the top and bottom surfaces of these samples. Pure PDMS controls were prepared by mixing Sylgard 184 components at a 10:1 volume ratio and curing at 60 °C for 24 h.

Compression testing was performed on a Bose Electroforce 3200 device. A 2.5 N load cell was used for the hydrogels and aerogels, while a 440 N cell was applied for the PDMS and composite samples. At the start of the tests, the samples were pre-loaded until full contact was achieved with the compression plates. Crosshead speed was 0.2 mm/s for all tests. Static compression was performed in one cycle, while dynamic testing was accomplished in five cycles of loading and unloading, and each cycle was progressed to achieve an additional 0.5 mm compression. In both cases, data acquisition was continued until sample failure. Compressive elastic modulus, elongation, and strength at the break were acquired from the static compression results. Elastic modulus was estimated as a linear regression slope coefficient over 1% strain of the samples. Residual deformation under dynamic conditions was derived as a maximum strain value at which stress equaled zero. In conjunction with maximum loading strain, the residual deformation permitted an estimate of the degree of mechanical degradation after the dynamic cycling. All acquisitions were performed for three samples of each material type: hydrogel, aerogel, and PDMS or composite.

Fractography studies were conducted on the dynamically tested composite samples to confirm the nature of their failure mode. A SEM microscope (JSEM 6010LA) was used to acquire microscopic images of the fractured sample morphology. In addition, EDX mapping was performed to determine the influence of the PEDOT:PSS and PDMS phases on the nature of mechanical failure.

Electrical characterization

For electrochemical studies, the composites were embedded in paraffin and sliced using a microtome (Leica RM2255) into ~0.5 mm to 1 mm thick films and cut to form 5×11 mm^2 rectangular pieces. A silver paste diluted with acetone was used to apply a conductive coating to the sample ends. A defined mask was applied to ensure that the silver paste was constrained to the samples' edges. Platinum controls were cut out of the 0.1 mm thick sheet with similar rectangular shape and dimensions.

Electrochemical impedance spectroscopy (EIS) and cyclic voltammetry (CV) measurements were performed on the AUTOLAB potentiostat–galvanostat (Multi Autolab/M101, Eco Chemie, The Netherlands), controlled by the preprogramed NOVA 2.0 software. EIS was conducted under sinusoidal voltage conditions at 0.1 Hz–100 kHz frequency range, followed by 11 cycles of CV within the potential window of −0.6 V to 0.8 V vs Ag/AgCl at a scan rate of 0.15 V/s. The final CV cycle was used for characterization assuming that the materials' performance was stabilized during the first ten cycles.

CE composites were placed in a wet cell to form the working electrode (WE). Platinum (Pt) was used as the counter electrode. Pt controls were mounted in the same conformation. The charge storage capacity (CSC) of the samples was measured as an area under the CV hysteresis (Cogan, 2008). Three composite samples from three batches (9 in total) and three platinum controls were characterized. The EIS/CV results were normalized with respect to the sample surface area submerged in phosphate buffered saline (PBS).

Dry cell tests utilized a two-electrode setup enabling current flow through the sample bulk. The CE composites were connected to the potentiostat with metallic clamps, while two wires were fixed in the aerogel for the connection. The sample conductivity was acquired at 1 kHz in the frequency domain and as a slope coefficient of nearly linear current/voltage relationship of the CV. The following equation was used for the conductivity (σ) calculation:

$$\sigma = \frac{L}{R \times A}, \tag{1}$$

where L is the distance between the clamps or the wires, A is the cross section area of the samples perpendicular to the current flow, and R is the impedance as recorded. The samples were measured twice, both with and without a conductive silver paste. 1 kHz was chosen as a typical characteristic frequency for the testing of bioelectrodes, enabling comparison to the literature. Three samples from three batches (9 in total) were used for characterization. A reference resistor with known impedance was used prior to each test to ensure the quality of connections and data acquisition.

For the electromechanical studies, cylindrical composite samples were used. Samples were subjected to ten cycles of dynamic compression down to 5%, 10%, 15%, and 20% strain on a MultiTest 5-xt Mecmesin device. Samples with no pre-load were used as controls. After the dynamic loading, samples' dry EIS conductivities (at 1 kHz) were measured. Three samples per type were used with an average size of 13 mm in diameter and 5 mm in thickness.

Calculation of PEDOT:PSS content

Hydrogel solid content (SC) shows the percentage of PEDOT:PSS within the initial PEDOT:PSS polymer network. This network comprises the body of the material and is not washed out upon contact with DI water or other solvents. To calculate the SC, six samples were weighed after the purification step ($m_{swollen}$), freeze-dried, and weighed again (m_{dried}). The SC was determined by the

following equation:

$$SC = \frac{m_{dry}}{m_{swollen}} \times 100\%. \quad (2)$$

The CP content (CPC) of the CE composites was determined as the PEDOT:PSS weight ratio present in the final CE material. It was assumed that the sample matrix volume was constant during the fabrication, and the CPC was calculated from the hydrogel SC and the volumetric density of DI water (ρ_w), air (ρ_a), PDMS (ρ_p), and hexane (ρ_h). This was achieved by representing the mass of the first matrix—DI water—as part of the hydrogel mass, using SC. All other matrices, used during the composite fabrication: air, 40 wt. % hexane/PDMS solution, and finally PDMS/air (assuming hexane was replaced by air upon evaporation)—were also represented via the initial hydrogels' mass and the density ratios. As a result, the unknown hydrogel mass was eliminated, and the following equation was derived (SC was presented as decimals and divided by 100%):

$$CPC = \frac{SC}{SC + \frac{(1-SC)}{\rho_w\left(\frac{0.4}{\rho_h} + \frac{0.6}{\rho_p}\right)}\left(0.4\frac{\rho_a}{\rho_h} + 0.6\right)} \times 100\%. \quad (3)$$

The densities used were: 997 kg/m^3 for DI water; 1.2 kg/m^3 for air; 659 kg/m^3 for hexane, and 1027 kg/m^3 for PDMS. The CPC was calculated for each of the six samples individually, and then, mean and standard deviation (SD) were obtained from resultant values.

Statistical analysis

All data are presented as values of mean ± standard deviation (SD). For electrochemical analysis, where three batches were used, the results are shown as pooled mean ± pooled SD. Since each batch has included an equal number of samples, the pooled mean was calculated as an arithmetical average of the batches' means, while Eq. (4) was used for the pooled SD (Cohen, 1998),

$$SD_{pooled} = \sqrt{\frac{SD_1^2 + SD_2^2 + SD_3^2}{k}}, \quad (4)$$

where SD_n is the SD of the corresponding batch and $k = 3$ is the number of batches. Since Eq. (4) is applicable only under homogeneity of variance assumption, the Levene test was conducted to ensure the variance equality across the batches. The test has found no significant difference between the variances under the significance level of $\alpha = 0.05$. The Levene test was chosen over the Bartlett test, as the sample size of 3 units was too small to determine the normality of the distribution.

Statistical analysis was performed to evaluate the electromechanical data. One-way ANOVA with Tukey post-hoc comparison was used to compare all data for 0% strain measurement and separately "no pre-load" and "20% pre-load" data across the 0%–20% strain range. One-way ANOVA without the post-hoc test was used to compare "no pre-load" and "20% pre-load" data at each strain point. Finally, two-way ANOVA with the Tukey test was used to simultaneously evaluate all "no pre-load" and "20% pre-load" data across the 0%–20% strain range. The "no pre-load" and "20% pre-load" data for the one-way and two-way ANOVA with the Tukey test were normalized by logarithmization. The normality and variance homogeneity of all data were checked with Shapiro–Wilk and Levene tests, respectively. All statistics were conducted at the significance level of $\alpha = 0.05$.

RESULTS AND DISCUSSION

Structural analysis of hydrogels and composites

Figure 2 shows the production of these CE composite materials and their microscopic structure. As imaged by SEM in Figs. 2(b)–2(e), the PEDOT:PSS aerogels exhibited an irregular, highly porous structure, with pore sizes exceeding 0.5 mm. The structure is anisotropic, forming horizontal continuous layers connected with vertical walls. The thickness of the layers and the walls was approximately the same and does not exceed 10 μm. As can be seen in Figs. 2(d) and 2(e), the PDMS has formed a continuous matrix around these thin PEDOT:PSS features. With an approximate size of 1 μm–10 μm, these PEDOT:PSS features correspond to the thickness of the aerogel layers and walls. EDX analysis further confirms that sulfur [purple in Fig. 2(e)] is predominately located within these features, surrounded by a material characterized by the presence of silicon. Thus, the composite structure consists of the thin PEDOT:PSS network embedded in the PDMS bulk matrix.

Large pores, seen in Fig. 2(d) on the edge of the composite, are defects that may affect the mechanical properties. Hexane is added to the PDMS to facilitate matrix penetration of the aerogel, and it has been hypothesized that pores may appear due to PDMS shrinkage during hexane evaporation. These pores have been successfully removed by curing the composite in a hexane/PDMS bath. Such an approach allows the PDMS from the bath to fill in the voids left as the hexane evaporates and ensures that the pores do not contribute to the electrical performance of the composite. Similar pores have appeared in the bulk of the composite when the hexane extraction conditions were too severe, for example, high temperatures or vacuum. Thus, hexane boiling environments or prolonged vacuuming should be avoided when forming composites in this way.

The hydrogel solid content (SC) and composite CP content (CPC) of the materials are illustrated in Fig. 3. The low SC of the hydrogel (0.92% on average) corresponds well with the highly porous structure observed in Fig. 2(b). This reflects a high amount of water content and suggests that the gelation protocol can be modified to increase the polymer SC. The estimated CPC was almost twice as high as the hydrogel SC, reaching 1.81% on average. This significant difference can be ascribed to the shrinkage of the hydrogel network during drying (which effectively starts as the hydrogel SC and becomes CPC once the PDMS is introduced). This is largely defined by using wt. % as a metric where a volumetric change has occurred. However, this is an intrinsic effect of the fabrication process and, hence, alters the density of the conductive component within the final material. Another factor may be the evaporation of hexane which initially occupies 40 wt. % of the hexane/PDMS matrix mass. This leads to a perceived rise in the PEDOT:PSS weight ratio in the composite as the volatile hexane evaporates. If the PDMS is able to continually flow through the composite during curing, it is possible that the entire structure could be filled, eliminating the voids. In this situation, the lowest possible CPC (or a ratio of CP to PDMS) would be achieved.

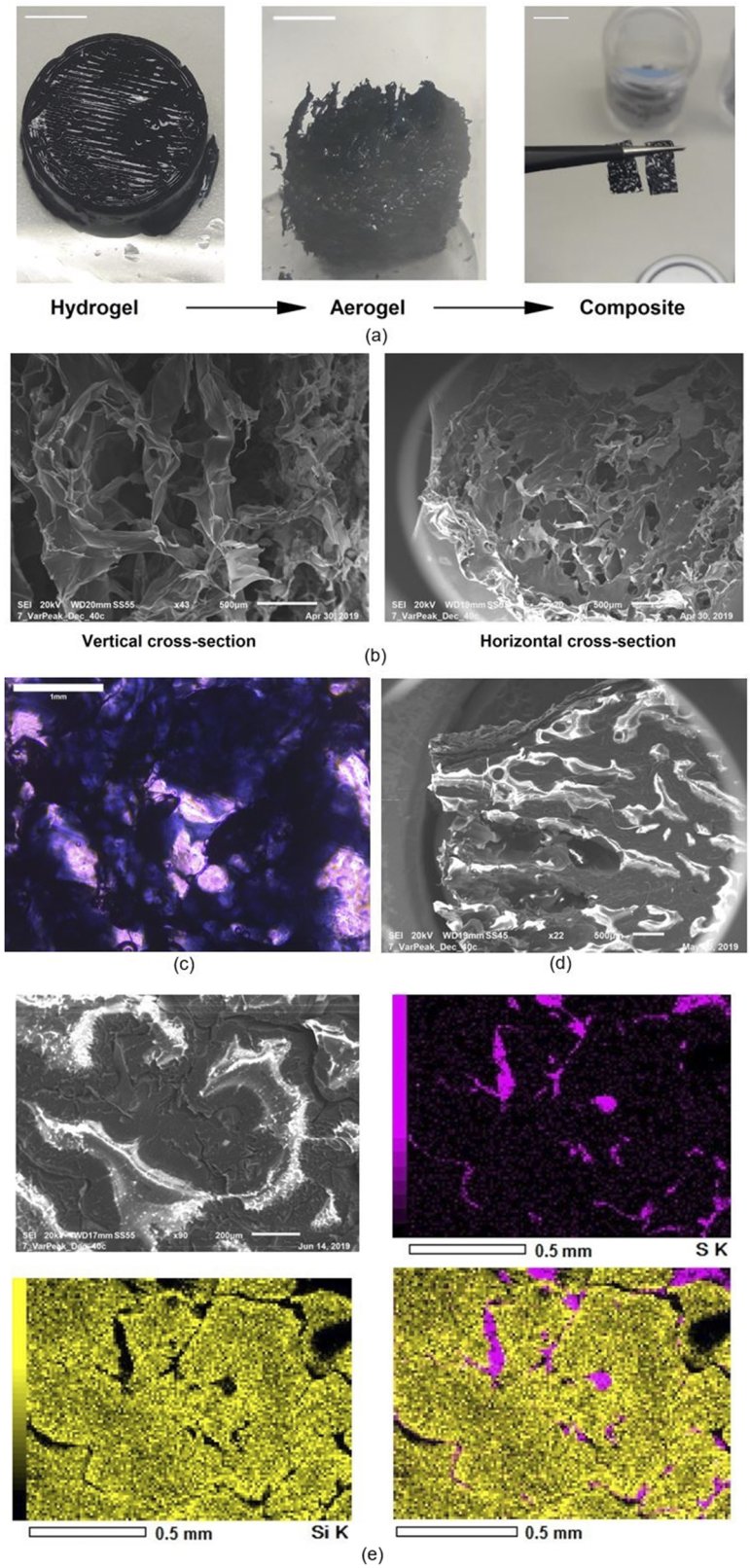

FIG. 2. Multi-scale images of the resultant materials. (a) Macroscopic photos of the materials given in the fabrication process order. Scale bars, 5 mm. (b) SEM images of the aerogels' cross sections. Upward wall remnants can be seen on the horizontal cross section. (c) Optical image of the composite. Transparent PDMS allows us to see the distribution of PEDOT:PSS in the bulk. (d) SEM image of the composite's vertical cross section. White stains are artifacts that have appeared due to the charging of insulative PDMS. No charging effect is seen around the PEDOT:PSS components. (e) EDS analysis of the composite's cross section surface. SEM image of the scanned area (upper left), sulfur (purple) distribution map (upper right), silicon (yellow) distribution map (lower left), and overlayered image of the maps (lower right).

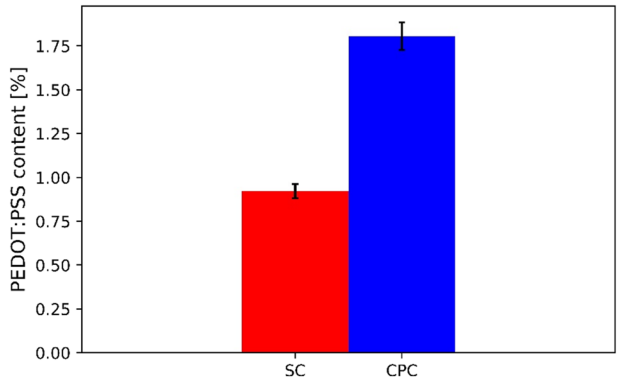

FIG. 3. Hydrogel SC and composite CPC as calculated by Eqs. (2) and (3). The discrepancy between the values estimates how the PEDOT:PSS weight ratio will change if the water "matrix" is replaced by PDMS.

The structure achieved by hydrogel templating exhibited promising features. Unlike the secondary PAA hydrogel network of Feig *et al.* (2018), the elastomer is formed within the PEDOT:PSS aerogel with an apparently continuous matrix structure. In conjunction with low CPC, it was expected that the elastomeric properties of the composite would be well preserved. The composite also maintains the interconnected PEDOT:PSS network from the aerogels. This network has the potential to reach relatively high conductivities despite the low CPC.

Mechanical characterization

Static compression results show that the PEDOT:PSS–PDMS composite mechanical behavior is quite similar to that of PDMS alone [Fig. 4(a)]. Additionally, the composite compressive strength and elastic modulus are far superior than those of the aerogels alone. This supports the hypothesis that the PDMS matrix can reinforce the conductive network. However, the discrepancy between the PDMS and the composite stress–strain curves also reveals that the PEDOT:PSS phase acts like a defect within the PDMS matrix. The compressive strength of the hydrogel alone and elongation at the break were lower than those previously reported by Yao *et al.* (2017) for aerogels, but of a similar order of magnitude: ~1.1 kPa vs 3.5 kPa and 15% vs 30%, respectively.

The elastic modulus of the CE composite was significantly lower than that of pure PDMS, as shown in Fig. 4(c). The opposite outcomes have been reported in the literature for the tensile loading of CP-filler composites, which have exhibited an increasing stiffness with higher CP content (Cuttaz *et al.*, 2019; Patton *et al.*, 2016). Such divergence in behavior may be ascribed not only to the different loading modes but also to the continuous nature of the aerogel network. A crack, formed at the PEDOT:PSS–PDMS interface, can propagate freely along the interface through the bulk of the material. At the same time, similar cracks in CP-filled composites should be localized, allowing a CP particle to contribute its strength to the composite mechanical behavior.

To determine the degree of elastomeric behavior enabled by the composite, dynamic compression was performed. As can be seen in Fig. 5(a), composite samples exhibit much greater divergence with each cycle than pure PDMS controls. Additionally, the increased area under the stress–strain curves indicated a higher energy dissipation. Together, these features imply that the CE composite displays a viscoelastic, rather than intrinsically elastic nature. Further quantification [Fig. 5(b)] reveals that the residual strain within the composite, on average, exceeds that of the neat PDMS by almost tenfold. This is despite both materials having a similar maximum loading strain across the last cycle. These data suggest that the presence of the PEDOT:PSS phase imparts plastic behavior to the PDMS matrix. The aerogels have been shown to be highly plastic, as depicted in Fig. 4(a), but they have a substantially lower modulus than the PDMS. Despite the CP comprising only 1.8 wt. % of the material composite, it is likely that this component is the point of initial failure, and subsequent irreversible deformation accumulates at the PEDOT:PSS–PDMS interface, in the form of delamination cracks.

To confirm the occurrence of the delamination, SEM/EDX fractography has been performed (Fig. 6). As illustrated in Fig. 6(a), the sample fracture image exhibits numerous sites of broadly opened PEDOT:PSS, unlike the thin, confined areas of PEDOT:PSS, shown in Fig. 2(e). A likely explanation for such broad areas of PEDOT:PSS on the fracture surface is that the cracks have propagated along the CP component rather than through it. Additionally, a clear site of interphase delamination has been observed [Fig. 6(b)] further supporting the proposed mode of failure from compression testing data.

Several possible enhancement routes are proposed for addressing the interfacial mismatch between the polymer components. A probable origin of delamination is PDMS non-polarity, which can cause poor adhesion between PEDOT:PSS and the supporting matrix. Thus, a general strategy for improvement is strengthening of the interphase adherence forces. One of the most straightforward ways to accomplish this is choosing matrix materials with higher polarity, such as polyurethane (PU) (Akindoyo *et al.*, 2016; Friedrich *et al.*, 2005; and Jaudouin *et al.*, 2012). PU ionomers, developed for biomedical applications, are of particular interest for further studies because of the ionic backbone groups that may reinforce the interface through ionic interactions with PEDOT:PSS. This is in addition to the standard Van der Waals intermolecular forces (Akindoyo *et al.*, 2016; Jaudouin *et al.*, 2012). Alternatively, other methods capable of reinforcing interfaces include matrix functionalization with polar groups, for example, ethylene oxide, or utilization of surfactant intermediate layers (Friedrich *et al.*, 2005; Noh, 2014). Finally, chemical cross-linking has the potential to create the strongest interface bonds; however, it has been previously shown with (3-glycidyloxypropyl)trimethoxysilane (GOPS) that it can also lead to a decrease in conductivity (Håkansson *et al.*, 2017).

An alternative approach to increasing the interfacial bonding strength is to reduce the mechanical mismatch at the interface between phases. Since, the CP phase is prone to fracture, it would be reasonable to attempt to modify its mechanical properties to be closer to that of the matrix phase. The potentially applicable methods for such CP modification include implementation of cross-linkers or property enhancing additives within a CP (ElMahmoudy *et al.*, 2017; Guex *et al.*, 2017; Håkansson *et al.*, 2017; and Wang *et al.*, 2017). While these approaches can impart a degree of flexibility, the former technique has shown to decrease the CP conductivity, while

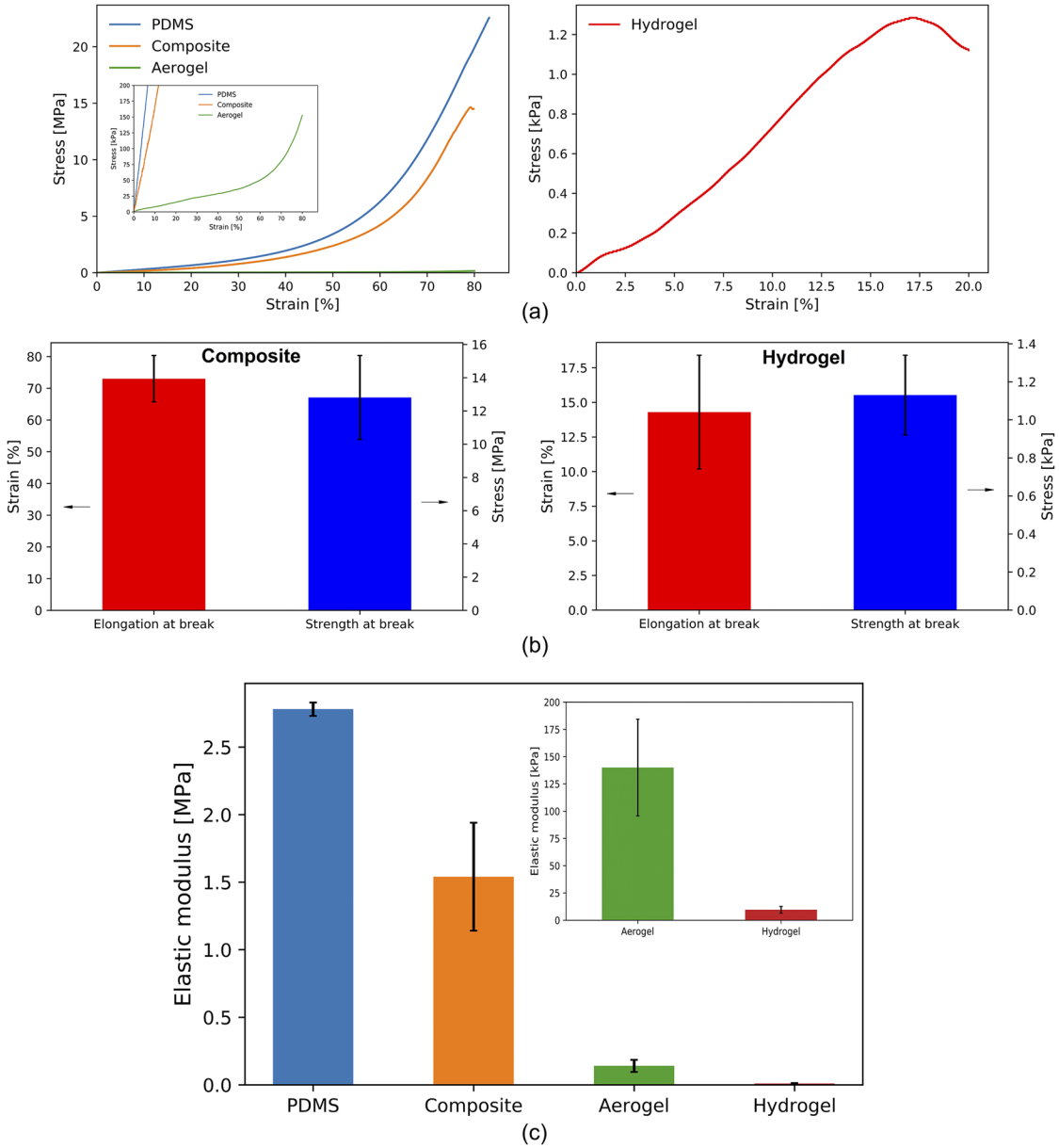

FIG. 4. Static mechanical behavior of the samples. (a) Stress–strain curves of PDMS, composites, and aerogels (left) and of hydrogels (right). The inset zooms the aerogels' stress–strain curve. (b) Elongation and strength at the break of the composites (left) and hydrogels (right). (c) Compressive elastic modulus of the samples. The inset zooms the aerogels' and hydrogels' results.

the results of the latter have exhibited poor mechanical behavior of a free-standing CP film upon repeat stretching (ElMahmoudy *et al.*, 2017; Håkansson *et al.*, 2017; and Wang *et al.*, 2017). The viscoelastic behavior of the film suggested that the additive strategy is applicable only in combination with an elastomeric supporting matrix (Wang *et al.*, 2017).

Flexible dopants, such as sulfonated polystyrene-block-poly(ethylene-ran-butylene)-block-polystyrene copolymer (SEBS), guar or xanthan gums, and glycosaminoglycans, may provide an alternative. However, the available studies have no comprehensive reports on mechanical properties of resultant materials, which have been mainly studied in terms of their electrical and biological characteristics (Barra *et al.*, 2004; Del Agua *et al.*, 2018; 2017; Mantione *et al.*, 2017; and 2016). Barra *et al.* reported that sulfonation of SEBS causes degradation of its mechanical properties (Barra *et al.*, 2004). Finally, gels fabricated from less rigid CP variants, such as PANI,

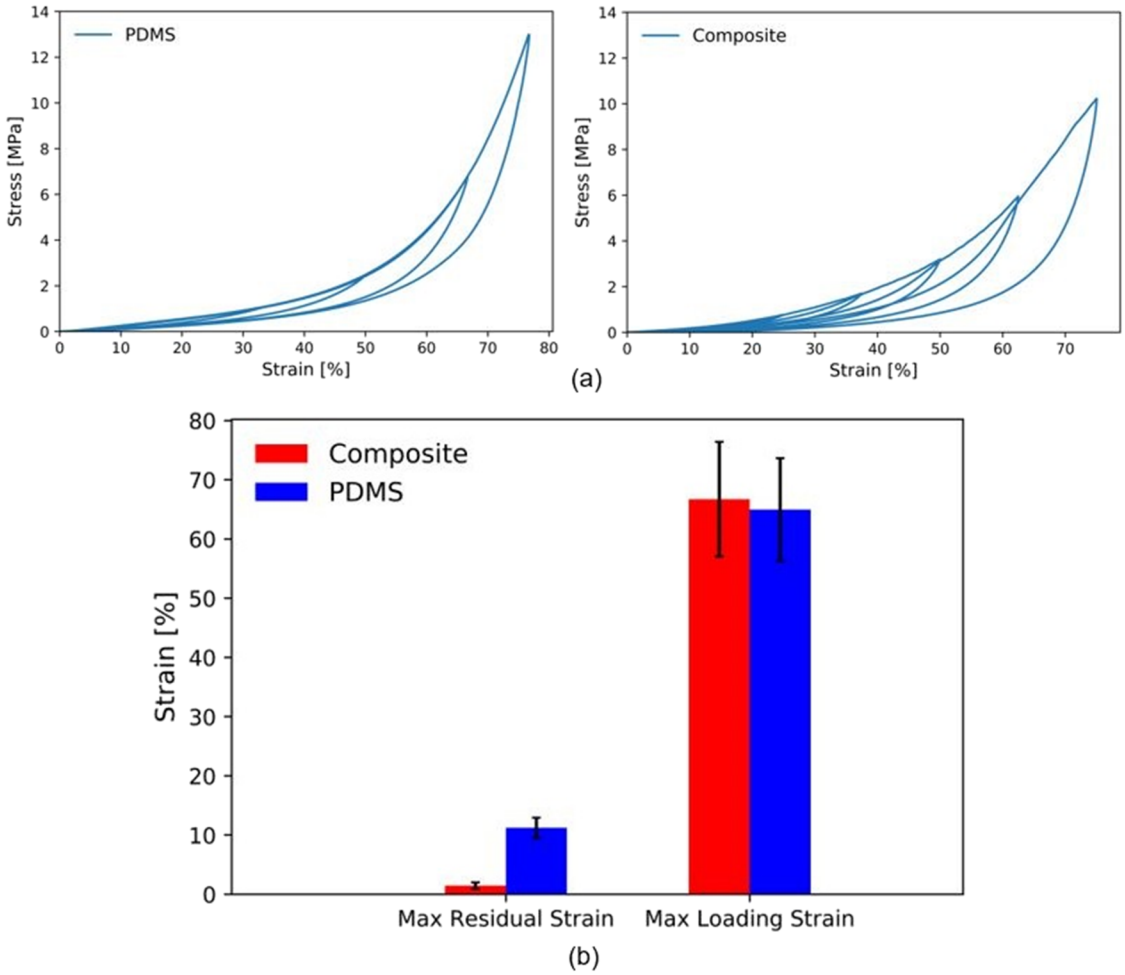

FIG. 5. Dynamic mechanical behavior of the samples. (a) Stress–strain curves of pure PDMS (left) and composites (right) under five cycles of repetitive compression. Arrows indicate the cycling progression. (b) Maximum loading deformation at the end of the last cycle and maximum irreversible, residual deformation, achieved by the samples.

may provide a mediating effect (Jana and Nandi, 2000; Pan *et al.*, 2012; Patton *et al.*, 2016; and Snook *et al.*, 2011).

Although the PDMS matrix has substantially reinforced PEDOT:PSS aerogels, the composite mechanical behavior is not truly elastomeric. The CP/matrix interface acts as a defect introducing a favorable path for crack propagation via delamination. As a result, the material becomes considerably weaker and accumulates greater residual strain upon repetitive stretching. Thus, the potential approaches for improvement should concentrate on enhancing the interphase adhesion and diminishing the mechanical mismatch between phases.

Electrical characterization

Highly conductive behavior is another crucial parameter for a genuine CE. To evaluate the electrical properties of the composites, EIS and cyclic voltammetry (CV) were performed. The studies were conducted in PBS electrolyte (wet cell) and dry ambient atmosphere (dry cell). In addition, the effect of hexane exposure and sample topography on composite conductivity was examined.

Wet cell studies were used to understand the capacity of the CE composite to inject charge within an aqueous environment, for example, when used as an electrode (in either pacemakers or bionic devices). These studies revealed that the composite electrochemical properties significantly differ from those of platinum controls. The platinum impedance spectrum (Fig. 7) exhibits well-defined capacitive behavior, acting like a high pass filter, whereas the composite response is more stable and resistive, showing a less frequency dependant impedance profile. Though the composite shows lower impedance at low frequencies, the platinum retains a superior charge transduction above the characteristic frequency of 1 kHz. This can be attributed to the higher ohmic conductivity of the platinum which supports a less resistive system once the capacitive behavior is overcome.

The phase spectra of the materials (Fig. 7) demonstrate more complicated charge transfer behavior. Platinum electrodes

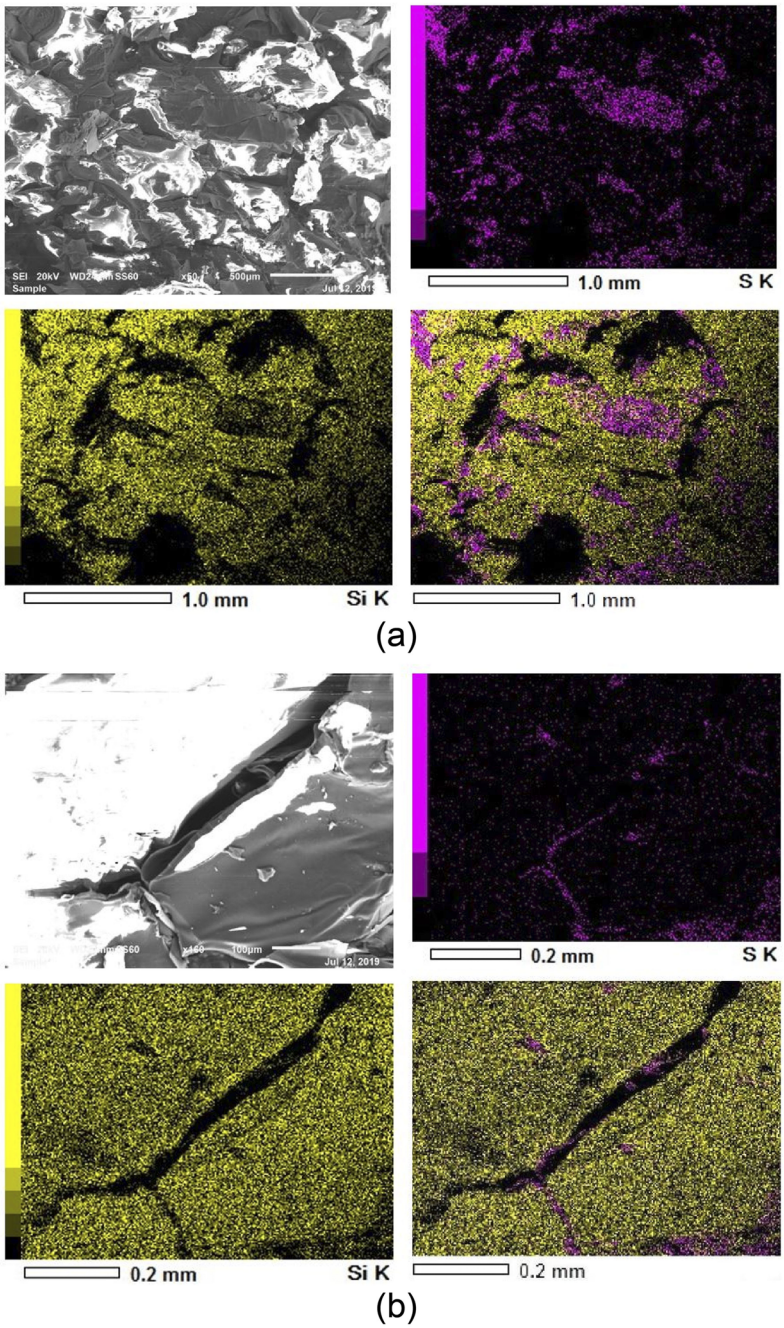

FIG. 6. SEM-EDS fractographical images. (a) A fracture site, showing wide sulfur phase areas (purple), corresponding to PEDOT:PSS. (b) A delamination site, showing a PEDOT:PSS sheet detaching from the PDMS matrix, as a crack forms.

experience an ~−80° depression near 30 Hz, the limiting frequency of their high pass behavior. Thus, this feature can be attributed to the typical platinum capacitive behavior, corresponding to the impedance magnitude spectrum (Cuttaz *et al.*, 2019; Green *et al.*, 2013). The high-frequency phase angle decrease can be attributed to the double layer on the electrode/electrolyte interface accumulating charge as the frequency drops. As a result, more potential is required to overcome the negative and positive charge attraction, leading to a current signal lag. By 30 Hz, the double-layer "capacitor" gathers enough charge to stabilize under working potential magnitude and begins to actively drain the circuit from the charge carriers, seemingly increasing the resistance. Alternatively, the process can be seen in terms of double-layer rearrangement requiring more energy as the opposing charges accumulate. As the phase lag further increases with

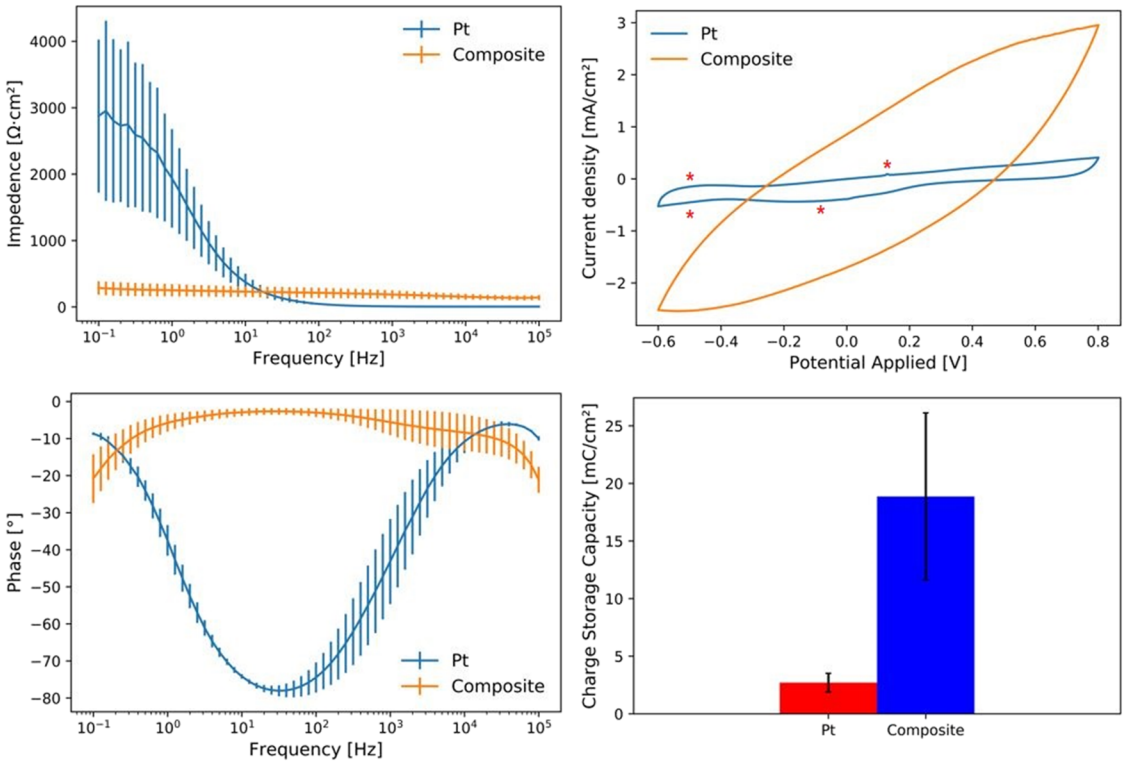

FIG. 7. Wet cell study results. EIS results are shown as impedance (upper left) and phase angle (lower left) frequency spectra. CV measurements are presented as surface current density over applied potential (upper right) and surface CSC (lower right) calculated as described above. Red asterisk mark peaks attributed to the platinum's redox reactions.

frequency drop and approaches the theoretical −90° threshold, the potential and current waveforms begin to synchronize due to their sinusoidal character. The CE composite phase behavior was more linear than that of platinum and is typical of PEDOT and other CP based materials (Cuttaz *et al.*, 2019; Kim *et al.*, 2018; and Tondera *et al.*, 2019). Its flat, near-zero pattern corresponds well with its considerably less capacitive impedance spectrum. However, a decline in the phase angle can be seen at low and high frequencies. Hypothetically, the low frequency response can be attributed to the slowly, but gradually, increasing influence of the double-layer charging, similar to the platinum. At high frequencies, the CP's relatively low charge carrier mobility may be the reason for the small current delays that produce a downturn in the phase response above 10 kHz.

The CV measurements also show the difference between the elastomer composite and platinum behavior. PEDOT:PSS–PDMS was observed to have a considerably larger hysteresis curve when compared to platinum. This supports their higher CSC (Fig. 7) and in functional electrode studies can lead to a high charge injection limit, such as those previously reported for CEs (Cuttaz *et al.*, 2019). The CSC also concurs with the EIS response, as Cogan has previously reported that materials with higher CSC exhibit decreased impedance at low frequencies (Cogan, 2008). The broader hysteresis suggests that faradaic charge injection mechanisms may occur in addition to the double-layer charging, in agreement with the previously reported conclusions of PEDOT:PSS being a pseudocapacitor (Cogan, 2008; Cuttaz *et al.*, 2019). Platinum can also display pseudocapacitive behavior (Cogan, 2008); however, this is highly dependent on the electrochemical potential. The faradaic redox reactions that give rise to pseudocapactivie behavior only occur at limited potential ranges (Cogan, 2008). The peaks of these reactions can be seen on the platinum CV plot at ∼−0.5 V, −0.1 V, and 0.1 V (Fig. 7, red asterisk). The PEDOT:PSS–PDMS plot does not exhibit any distinguishable peaks, suggesting that the peaks associated with the redox chemistry are smaller and, hence, masked by the larger non-faradaic charge transfer response. Cogan (2008) proposed that for PEDOT, the capacitive double layer may be the prevailing mechanism above −0.6 V (Ag|AgCl), which would also correspond with the absence of peaks. In that case, a broader hysteresis can potentially originate from a higher active surface area imparted by the presence of the CPs (Cogan, 2008; Cuttaz *et al.*, 2019). Since the platinum and elastomer composite samples were approximately of the same size and the electrically active PEDOT:PSS comprised only 1.8 wt. % of the composite, the superior CSC is even more outstanding. However, it may be difficult to quantify the intrinsic active surface of the composite as the electrolyte may leak between the PEDOT:PSS and PDMS due to the delamination cracks between the two phases.

Profilometry results indicate that the PEDOT:PSS–PDMS surface was generally flat with numerous thin cavities about 0.4 mm

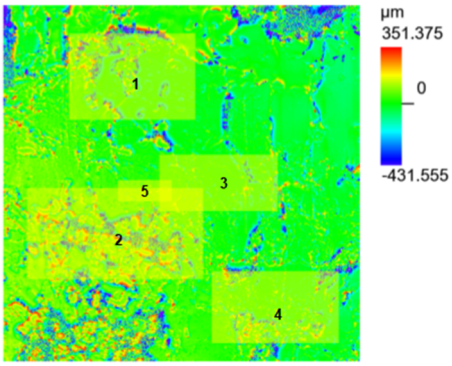

FIG. 8. Topographical map of a composite slice, showing height distribution on the sample's surface. Blue wall structures (PEDOT:PSS) can be seen on the green flat background (PDMS). Five areas are selected, and their arithmetical mean height is presented in Table I.

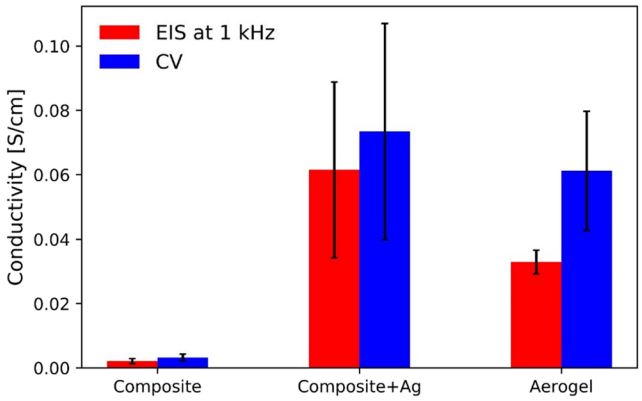

FIG. 9. Conductivity values of composite, silver paste connected (Ag) composite and as-prepared aerogel samples. The results have been obtained using the dry cell setup.

deep (Fig. 8). Such a structure supports the observations from SEM, where the PEDOT:PSS phase exhibited a thin network of walls within the PDMS. It can be hypothesized that the mechanical mismatch and delamination during the microtome slicing of samples may result in the CP being recessed within the PDMS at the edges. In fact, red areas of elevations can often be seen around these thin blue structures. These may be agglomerations of PEDOT:PSS or of PDMS, appearing due to plastic deformation of the former. Irrespective of their origin, they cause higher roughness than the rest of the surface (Table I, Area 2 vs 5). As a result, such roughness or particulate around the exposed conductive network could impact on lead connection and cause decreased electrical performance during data acquisition for CV and EIS.

Dry cell conductivity studies are presented in Fig. 9. These are used to establish the conductivity within the CE composite material, which will be critical to determining the potential use as a lead wire. Initial measurements used metal connectors to the interface with the outer surface of the composite. This led to unexpectedly low values of conductivity. In subsequent studies, silver (Ag) paste was applied at the distal ends of the samples to ensure connection to the bulk material inside the composite construct. The studies demonstrate that once the effective connection is made to the sample, by contacting the PEDOT component within the bulk, substantially higher conductivities are obtained. This is achieved when the paste fills the cavities, supporting the prior supposition from profilometry that the PEDOT:PSS phase is recessed within the PDMS when the sample is cut to expose a cross section. The values reached with the silver paste connection are close to the conductivity of the neat aerogels (Fig. 9). This suggests that the gel network resistance is not affected considerably during the composite formation. Regardless, both measurements of composite conductivity (connecting to the outer surface and the cross sectional bulk) are significantly higher than those of PDMS alone. This increase in conductivity by more than 10 orders of magnitude [PDMS has a conductivity of $0.25 * 10^{-15}$ S/cm (Mark, 1999)] supports the hypothesis that a PEDOT:PSS template can maintain a connected network when formed into a composite with an insulative elastomer.

TABLE I. Arithmetical mean height of the areas selected in Fig. 8.

Area (№)	Sa (μm)
1	66.947
2	99.742
3	28.675
4	55.049
5	18.876

The composite conductivity was compared to similar material systems reported in the literature (Cuttaz *et al.*, 2019; Lu *et al.*, 2019; Seyedin *et al.*, 2014; Yao *et al.*, 2017; and Yuxin *et al.*, 2018). As illustrated in Fig. 10, the values obtained for this study (red squares) are considerably lower when compared to most of the conventional composites presented in the literature [blue circles, (Cuttaz *et al.*, 2019; Seyedin *et al.*, 2014)]. However, it must be considered that these samples only contained 1.8 wt. % CP. All other reports of conductivity for CP composites have used substantially higher CP loadings (ranging from 5 wt. % to 25 wt. %) and most show a linear relationship above their percolation threshold. The increased amount of CP in these prior composites should lead to a greater number of conductive pathways and correlate with increased bulk conductivity. However, it is possible to extrapolate from these data that the low CPC of the composites reported herein could achieve a significantly higher conductivity, plotted as the potential (Fig. 9, black diamonds). Equation (3) was applied with reference to the solid content values of the previously reported aerogels to evaluate the expected conductivity of composites formed by adding a PDMS matrix to these gels (Lu *et al.*, 2019; Yao *et al.*, 2017; and Yuxin *et al.*, 2018). As a result, it can be expected that increasing the CPC of the gel composites will be a viable strategy for improving material electrical properties. However, increasing the CPC of these composites is a fine balance between the various desired properties. Increased CPC can cause further degradation of the mechanical properties, and thus, an optimal CPC value must be found. Hansen *et al.* achieved very high conductivity with loadings in the range of 30 wt. %–50 wt. % CPC with PEDOT:*p*-tosylate/PU composites;

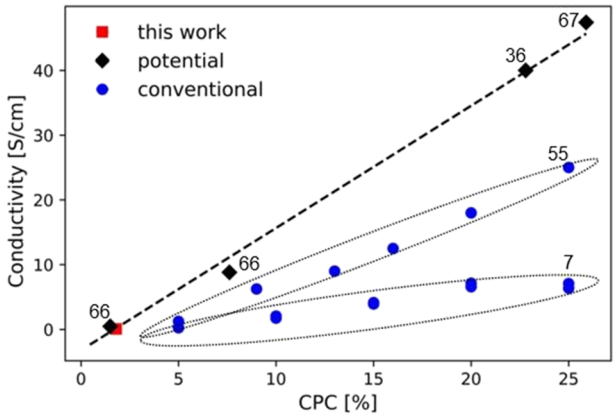

FIG. 10. Conductivities of composites developed in this and previously reported studies. All values were distributed among three groups. The first group includes the result stated above for the CE composites (red squares). The second (blue circles)—achieved by the conventional methods—uses CP particles to create interpenetrating networks inside an elastomer matrix (Cuttaz *et al.*, 2019; Seyedin *et al.*, 2014). The last group (black diamonds) consists of the values that can potentially be achieved by using the hydrogel template method with the hydrogels reported in the papers (Lu *et al.*, 2019; Yao *et al.*, 2017; and Yuxin *et al.*, 2018). The dashed line shows an estimated linear relationship between the gel composite conductivity and CPC.

however, the paper does not report any stress–strain behavior of the material (Hansen *et al.*, 2007).

The SC of the initial hydrogel may also prove challenging to increase, while still enabling penetration of the elastomeric secondary matrix. For CP-filled composites, simply adding more CP is relatively straightforward, but for the gel template system, new and more complex hydrogel fabrication techniques may be required. This could diminish the processability and cost-effectiveness of the hydrogel templating. It is possible that gains in conductivity may be made by combining the CP-filled and templated composite approaches. In addition, the hydrogel template method currently uses polymeric dopant ions, such as PSS, to form an aqueous dispersion of the PEDOT:PSS prior to gelling. In contrast, filler methods can use PEDOT particles with small dopant ions, such as tosylate, incorporated using organic solvents (Hansen *et al.*, 2007). This results in a CP product that can be purified and reduces the insulative effect caused by the excess dopant. Thus, gel purification steps or dopant modification may provide an alternate approach for achieving higher conductivities.

Plotting a similar graph for electromechanical behavior dependence from the CPC would be difficult due to lack of data. However, for the reported cases, the conductivity is usually stated to be indifferent from the applied strain (Lu *et al.*, 2019; Yuxin *et al.*, 2018). Thus, it can be suggested that the conductivity/CPC plot should also remain the same at the reported 0%–20% strain range. In addition, at this strain range, the gel composite dynamic stress–strain curve does not exhibit a broad hysteresis [Fig. 5(a)]. Thus, the mechanical effects on the conductivity can be estimated as marginal due to relatively low amount of accumulated mechanical defects.

This hypothesis was further supported by the electromechanical study conducted on the gel composites. Figure 11 shows no considerable alteration of dry conductivity between cyclically pre-loaded and ordinary ("no pre-load") samples at different levels of strain. The statistical analysis of the data found no significant influence of the pre-load on the conductivity of the samples. However, it was found that conductivity of the "20% pre-load" samples tended to increase at larger static compression. "20% pre-load" one-way ANOVA and two-way ANOVA post-hoc comparisons indicated that conductivity increased considerably between 0% and 15% or 20% strains. This behavior is thought to be associated with the enhancement of contact between the samples and measuring electrodes as a result of surface flattening of samples' surface roughness and a larger contact area. Interestingly, no such statistical increase was found for the "no pre-load" samples, which may suggest a combined influence of the pre-load and measurement strain for the "20% pre-load" samples. However, the two-way ANOVA concluded a

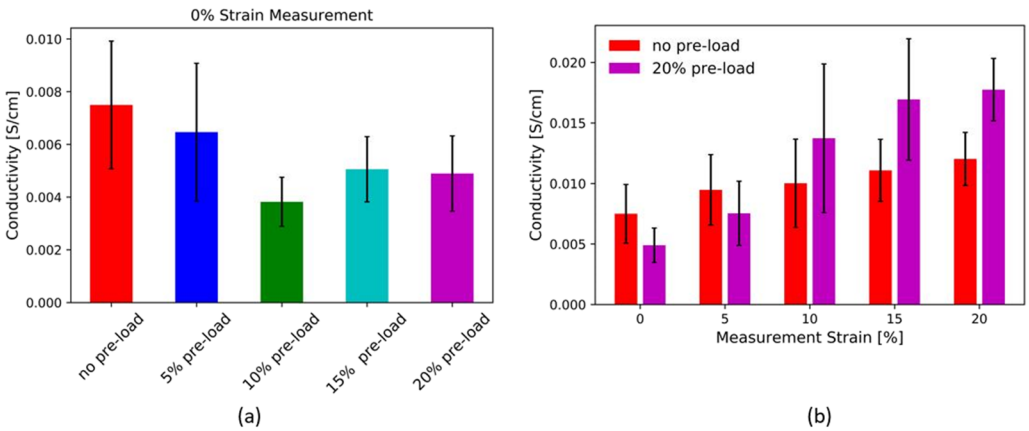

FIG. 11. Electromechanical behavior of the PEDOT:PSS–PDMS composites at solely 0% (a) and 0%–20% strain range (b). Dynamically pre-loaded samples are labeled "pre-load" with the corresponding pre-loading cyclic strain. Control samples that were not loaded prior to the conductivity measurements are labeled "no pre-load." (b) X-axis indicates static mechanical strain at which the dry conductivity measurements were taken.

p-value of 0.2 and an omega squared of 0.05 for the interfactoral interaction. This implies that even if the combined effect had taken place, it was only a marginal effect.

Overall, the electrochemical, electrical, and mechanical performances of these composites present a promising alternative strategy for fabricating polymer bioelectronics. The electrochemical analysis (in wet electrolyte conditions) demonstrates typical low impedance and high charge transfer seen in CP based materials, showing a clear benefit over platinum electrodes. The dry cell measurements have shown that once contact to the conductive phase is effectively established, composites generally exhibit conductivities reflective of the neat aerogels prior to the introduction of the insulative elastomer phase. These results suggest that estimates of increased conductivity through increasing CPC are valid. However, increasing CPC will not address the plastic deformation and crack propagation encountered at the component polymer interface. Similar phenomena have been observed in metallic particulate systems, such as silver nanowires (Mi *et al.*, 2014; Yang *et al.*, 2016), with approaches to mitigate this effect involving the introduction of complementary ionic groups to the elastomer component, improving adhesion between the two phases. Further improvements require a systematic approach, which considers electrical and mechanical parameters simultaneously. Additionally, although the PDMS and PEDOT:PSS materials that form the composite are commonly used for the design of biomedical devices and regarded as biocompatible, further cytocompatibility studies of this material are required.

CONCLUSION AND PERSPECTIVES

This study has introduced a method by which a fully polymeric CE composite is formed from a bulk elastomeric PDMS matrix and a continuous conductive PEDOT:PSS network. Such structures permit the fabrication of composites outside of the traditional percolation threshold paradigm. These CE composites exhibited a higher electrochemical performance at a lower CP content, with enhanced mechanical behavior when compared to metallic or neat CP systems used in electrode technologies. The fabricated samples have shown that the matrix mechanically supports the conductive phase, which is capable of conducting charge carriers under both wet and dry conditions with a CPC as low as 1.8 wt. %. These materials were shown to exhibit viscoelasticity via interphase delamination and relatively large electrical resistance, making them less ideal as lead technologies, such as those used in pacemakers and electrode array interconnects. However, with future refinement, this material fabrication technique has the potential to offer a simple method for the development of conducting polymer leads. Future research will concentrate on improving the interphase adhesion while optimizing CPC and conductivity.

AUTHORS' CONTRIBUTIONS

A.N., J.G., C.C., and R.A.G. conceptualized the study; A.N., J.G., C.C., E.C., and R.A.G. derived the methodology; A.N. and E.C. wrote the software; A.N. validated the study; A.N. performed the formal analysis and investigated the study; R.A.G. supplied the resources; A.N. wrote the original draft; A.N., J.G., C.C., and R.A.G. reviewed and edited the manuscript; A.N. conducted the project administration; J.G. and R.A.G. supervised the study; and A.N. and R.A.G. contributed to funding acquisition.

ACKNOWLEDGMENTS

The authors acknowledge the funding from the Healthcare Technologies Challenge Awards (HTCA) grant of the Engineering and Physical Sciences Research Council (EPSRC), No. EP/R004498/1, and the support of the EPSRC Centre for Doctoral Training in Plastic Electronics, Imperial College London. Alexey Novikov would like to express gratitude to Leonid and Larisa Novikov for support and funding of his postgraduate position. The authors thank Martina Genta for invaluable assistance in mechanical study design.

The authors declare no competing interests.

DATA AVAILABILITY

The data that support the findings of this study are available from the corresponding author upon reasonable request.

REFERENCES

Akindoyo, J. O., Beg, M. D. H., Ghazali, S., Islam, M. R., Jeyaratnam, N., and Yuvaraj, A. R., "Polyurethane types, synthesis and applications—A review," RSC Adv. **6**, 114453–114482 (2016).

Baek, S., Green, R. A., and Poole-Warren, L. A., "The biological and electrical trade-offs related to the thickness of conducting polymers for neural applications," Acta Biomater. **10**, 3048–3058 (2014).

Barra, G. M. O., Jacques, L. B., Oréfice, R. L., and Carneiro, J. R. G., "Processing, characterization and properties of conducting polyaniline-sulfonated SEBS block copolymers," Eur. Polym. J. **40**, 2017–2023 (2004).

Cogan, S. F., "Neural stimulation and recording electrodes," Annu. Rev. Biomed. Eng. **10**, 275–309 (2008).

Cogan, S. F., Troyk, P. R., Ehrlich, J., and Plante, T. D., "*In vitro* comparison of the charge-injection limits of activated iridium oxide (AIROF) and platinum-iridium microelectrodes," IEEE Trans. Biomed. Eng. **52**, 1612–1614 (2005).

Cohen, J., *Statistical Power Analysis for the Behavioral Sciences*, 2nd ed. (Lawrence Erlbaum, Hillsdale, 1998).

Cuttaz, E., Goding, J., Vallejo-Giraldo, C., Aregueta-Robles, U., Lovell, N., Ghezzi, D., and Green, R. A., "Conductive elastomer composites for fully polymeric, flexible bioelectronics," Biomater. Sci. **7**, 1372–1385 (2019).

Dai, T., Qing, X., Lu, Y., and Xia, Y., "Conducting hydrogels with enhanced mechanical strength," Polymer **50**, 5236–5241 (2009).

Dai, T., Qing, X., Zhou, H., Shen, C., Wang, J., and Lu, Y., "Mechanically strong conducting hydrogels with special double-network structure," Synth. Met. **160**, 791–796 (2010).

Da Silva, A. C., Semeano, A. T. S., Dourado, A. H. B., Ulrich, H., and Cordoba de Torresi, S. I., "Novel conducting and biodegradable copolymers with noncytotoxic properties toward embryonic stem cells," ACS Omega **3**, 5593–5604 (2018).

Del Agua, I., Mantione, D., Casado, N., Sanchez-Sanchez, A., Malliaras, G. G., and Mecerreyes, D., "Conducting polymer iongels based on PEDOT and guar gum," ACS Macro Lett. **6**, 473–478 (2017).

Del Agua, I., Marina, S., Pitsalidis, C., Mantione, D., Ferro, M., Iandolo, D., Sanchez-Sanchez, A., Malliaras, G. G., Owens, R. M., and Mecerreyes, D., "Conducting polymer scaffolds based on poly(3,4-ethylenedioxythiophene) and xanthan gum for live-cell monitoring," ACS Omega **3**, 7424–7431 (2018).

ElMahmoudy, M., Inal, S., Charrier, A., Uguz, I., Malliaras, G. G., and Sanaur, S., "Tailoring the electrochemical and mechanical properties of PEDOT:PSS films for bioelectronics," Macromol. Mater. Eng. **302**, 1600497 (2017).

Feig, V. R., Tran, H., Lee, M., and Bao, Z., "Mechanically tunable conductive interpenetrating network hydrogels that mimic the elastic moduli of biological tissue," Nat. Commun. **9**, 2740 (2018).

Ferreira, A. M., Costa, F., Marques, H., Cardim, N., Tralhao, A., and Adragão, P., "MRI-conditional pacemakers: Current perspectives," Med. Devices: Evidence Res. **7**, 115–124 (2014).

Friedrich, K., Fakirov, S., and Zhang, Z., *Polymer Composites: From Nano-to-Macro-Scale* (Springer, New York, 2005).

Fung, Y. C., *Biomechanics: Mechanical Properties of Living Tissues* (Springer Science & Business Media, 2013).

Goding, J., Vallejo-Giraldo, C., Syed, O., and Green, R., "Considerations for hydrogel applications to neural bioelectronics," J. Mater. Chem. B **7**, 1625–1636 (2019).

Green, R. A., Matteucci, P. B., Hassarati, R. T., Giraud, B., Dodds, C. W. D., Chen, S., Byrnes-Preston, P. J., Suaning, G. J., Poole-Warren, L. A., and Lovell, N. H., "Performance of conducting polymer electrodes for stimulating neuroprosthetics," J. Neural Eng. **10**, 16009 (2013).

Guex, A. G., Puetzer, J. L., Armgarth, A., Littmann, E., Stavrinidou, E., Giannelis, E. P., Malliaras, G. G., and Stevens, M. M., "Highly porous scaffolds of PEDOT:PSS for bone tissue engineering," Acta Biomater. **62**, 91–101 (2017).

Håkansson, A., Han, S., Wang, S., Lu, J., Braun, S., Fahlman, M., Berggren, M., Crispin, X., and Fabiano, S., "Effect of (3-glycidyloxypropyl) trimethoxysilane (GOPS) on the electrical properties of PEDOT:PSS films," J. Polym. Sci., Part B: Polym. Phys. **55**, 814–820 (2017).

Hansen, T. S., West, K., Hassager, O., and Larsen, N. B., "Highly stretchable and conductive polymer material made from poly(3,4-ethylenedioxythiophene) and polyurethane elastomers," Adv. Funct. Mater. **17**, 3069–3073 (2007).

Haqqani, H. M., Epstein, L. M., and Cooper, J. M., "Engineering and constraction of pacemaker and ICD leads," Clin. Gate (published online 2018), available at https://clinicalgate.com/engineering-and-construction-of-pacemaker-and-icd-leads-2/.

Hassarati, R. T., Goding, J. A., Baek, S., Patton, A. J., Poole-Warren, L. A., and Green, R. A., "Stiffness quantification of conductive polymers for bioelectrodes," J. Polym. Sci., Part B: Polym. Phys. **52**, 666–675 (2014).

Huang, T.-Y. and Baba, N., "Cardiac pathology of transvenous pacemakers," Am. Heart J. **83**, 469–474 (1972).

Jana, T. and Nandi, A. K., "Sulfonic acid-doped thermoreversible polyaniline gels: Morphological, structural, and thermodynamical investigations," Langmuir **16**, 3141–3147 (2000).

Jaudouin, O., Robin, J.-J., Lopez-Cuesta, J.-M., Perrin, D., and Imbert, C., "Ionomer-based polyurethanes: A comparative study of properties and applications," Polym. Int. **61**, 495–510 (2012).

Kalin, R. and Stanton, M. S., "Current clinical issues for MRI scanning of pacemaker and defibrillator patients," Pacing Clin. Electrophysiol. **28**, 326–328 (2005).

Kaur, G., Adhikari, R., Cass, P., Bown, M., and Gunatillake, P., "Electrically conductive polymers and composites for biomedical applications," RSC Adv. **5**, 37553–37567 (2015).

Kim, B. R., Lee, H. K., Park, S. H., and Kim, H. K., "Electromagnetic interference shielding characteristics and shielding effectiveness of polyaniline-coated films," Thin Solid Films **519**, 3492–3496 (2011).

Kim, S.-M., Kim, C.-H., Kim, Y., Kim, N., Lee, W.-J., Lee, E.-H., Kim, D., Park, S., Lee, K., Rivnay, J., and Yoon, M.-H., "Influence of PEDOT:PSS crystallinity and composition on electrochemical transistor performance and long-term stability," Nat. Commun. **9**, 3858 (2018).

Landers, R., Pfister, A., Hübner, U., John, H., Schmelzeisen, R., and Mülhaupt, R., "Fabrication of soft tissue engineering scaffolds by means of rapid prototyping techniques," J. Mater. Sci. **37**, 3107–3116 (2002).

Levine, G. N., Gomes, A. S., Arai, A. E., Bluemke, D. A., Flamm, S. D., Kanal, E., Manning, W. J., Martin, E. T., Smith, J. M., Wilke, N., Shellock, F. S., and Shellock, F. S., "Safety of magnetic resonance imaging in patients with cardiovascular devices," Circulation **116**, 2878–2891 (2007).

Li, P., Du, D., Guo, L., Guo, Y., and Ouyang, J., "Stretchable and conductive polymer films for high-performance electromagnetic interference shielding," J. Mater. Chem. C **4**, 6525 (2016).

Lo, W. W. M., "Imaging of cochlear and auditory brain stem implantation," Am. J. Neuroradiol. **19**, 1147 (1998).

Lu, B., Yuk, H., Lin, S., Jian, N., Qu, K., Xu, J., and Zhao, X., "Pure PEDOT:PSS hydrogels," Nat. Commun. **10**, 1043 (2019).

Luebben, S., Sapp, S., Sa, R. D., Elliott, B., and Ellis, W., "Solvent processable conducting block copolymers based on poly(3,4-ethylenedioxythiophene)," in 11th International Seminar on the Commercial Applications for Inherently Conductive Polymers, 2004.

Mantione, D., del Agua, I., Sanchez-Sanchez, A., Mecerreyes, D., Mantione, D., Del Agua, I., Sanchez-Sanchez, A., and Mecerreyes, D., "Poly(3,4-ethylenedioxythiophene) (PEDOT) derivatives: Innovative conductive polymers for bioelectronics," Polymers **9**, 354 (2017).

Mantione, D., del Agua, I., Schaafsma, W., Diez-Garcia, J., Castro, B., Sardon, H., and Mecerreyes, D., "Poly(3,4-ethylenedioxythiophene):glycosaminoglycan aqueous dispersions: Toward electrically conductive bioactive materials for neural interfaces," Macromol. Biosci. **16**, 1227–1238 (2016).

Mark, J. E., *Polymer Data Handbook*, 2nd ed. (Oxford University Press, New York, 1999).

Merrill, D. R., Bikson, M., and Jefferys, J. G. R., "Electrical stimulation of excitable tissue: Design of efficacious and safe protocols," J. Neurosci. Methods **141**, 171–198 (2005).

Mi, H.-Y., Li, Z., Turng, L.-S., Sun, Y., and Gong, S., "Silver nanowire/thermoplastic polyurethane elastomer nanocomposites: Thermal, mechanical, and dielectric properties," Mater. Des. **56**, 398–404 (2014).

Moore, D. R. and Shannon, R. V., "Beyond cochlear implants: Awakening the deafened brain," Nat. Neurosci. **12**, 686 (2009).

Noh, J.-S., "Highly conductive and stretchable poly(dimethylsiloxane):poly(3,4-ethylenedioxythiophene):poly(styrene sulfonic acid) blends for organic interconnects," RSC Adv. **4**, 1857–1863 (2014).

Nordbeck, P., Ertl, G., and Ritter, O., "Magnetic resonance imaging safety in pacemaker and implantable cardioverter defibrillator patients: How far have we come?," Eur. Heart J. **36**, 1505–1511 (2015).

Normann, R., "Technology insight: Future neuroprosthetic therapies for disorders of the nervous system," Nat. Clin. Pract. Neurol. **3**, 444 (2007).

Pan, L., Yu, G., Zhai, D., Lee, H. R., Zhao, W., Liu, N., Wang, H., Tee, B. C.-K., Shi, Y., Cui, Y., and Bao, Z., "Hierarchical nanostructured conducting polymer hydrogel with high electrochemical activity," Proc. Natl. Acad. Sci. U. S. A. **109**, 9287–9292 (2012).

Patton, A. J., Green, R. A., and Poole-Warren, L. A., "Mediating conducting polymer growth within hydrogels by controlling nucleation," APL Mater. **3**, 014912 (2015).

Patton, A. J., Poole-Warren, L. A., and Green, R. A., "Mechanisms for imparting conductivity to nonconductive polymeric biomaterials," Macromol. Biosci. **16**, 1103–1121 (2016).

Polikov, V. S., Tresco, P. A., and Reichert, W. M., "Response of brain tissue to chronically implanted neural electrodes," J. Neurosci. Methods **148**, 1–18 (2005).

Rivnay, J., Owens, R. M., and Malliaras, G. G., "The rise of organic bioelectronics," Chem. Mater. **26**, 679–685 (2014).

Rivnay, J., Wang, H., Fenno, L., Deisseroth, K., and Malliaras, G. G., "Next-generation probes, particles, and proteins for neural interfacing," Sci. Adv. **3**, e1601649 (2017).

Sasaki, M., Karikkineth, B. C., Nagamine, K., Kaji, H., Torimitsu, K., and Nishizawa, M., "Highly conductive stretchable and biocompatible electrode-hydrogel hybrids for advanced tissue engineering," Adv. Healthcare Mater. **3**, 1919–1927 (2014).

Sekine, S., Ido, Y., Miyake, T., Nagamine, K., and Nishizawa, M., "Conducting polymer electrodes printed on hydrogel," J. Am. Chem. Soc. **132**, 13174–13175 (2010).

Seyedin, M. Z., Razal, J. M., Innis, P. C., and Wallace, G. G., "Strain-responsive polyurethane/PEDOT:PSS elastomeric composite fibers with high electrical conductivity," Adv. Funct. Mater. **24**, 2957–2966 (2014).

Shepherd, R. K., Shivdasani, M. N., Nayagam, D. A. X., Williams, C. E., and Blamey, P. J., "Visual prostheses for the blind," Trends Biotechnol. **31**, 562–571 (2013).

Snook, G. A., Kao, P., and Best, A. S., "Conducting-polymer-based supercapacitor devices and electrodes," J. Power Sources **196**, 1–12 (2011).

Tahk, D., Lee, H. H., and Khang, D.-Y., "Elastic moduli of organic electronic materials by the buckling method," Macromolecules **42**, 7079–7083 (2009).

Tandon, N., Cannizzaro, C., Chao, P.-H. G., Maidhof, R., Marsano, A., Ting, H., Au, H., Radisic, M., and Vunjak-Novakovic, G., "Electrical stimulation systems for cardiac tissue engineering," Nat. Protoc. **4**, 155 (2009).

Timperley, J., Leeson, P., Mitchell, A. R., Mitchell, A. R., and Betts, T., "Pacemaker principles," in *Pacemakers and ICDs* (Oxford University Press, 2007), Chap. 1.

Tondera, C., Akbar, T. F., Thomas, A. K., Lin, W., Werner, C., Busskamp, V., Zhang, Y., and Minev, I. R., "Highly conductive, stretchable, and cell-adhesive hydrogel by nanoclay doping," Small **15**, 1901406 (2019).

Wang, Y. and Jing, X., "Intrinsically conducting polymers for electromagnetic interference shielding," Polym. Adv. Technol. **16**, 344–351 (2005).

Wang, Y., Zhu, C., Pfattner, R., Yan, H., Jin, L., Chen, S., Molina-Lopez, F., Lissel, F., Liu, J., Rabiah, N. I., Chen, Z., Chung, J. W., Linder, C., Toney, M. F., Murmann, B., and Bao, Z., "A highly stretchable, transparent, and conductive polymer," Sci. Adv. **3**, e1602076 (2017).

Yagci, Y. and Toppare, L., "Electroactive macromonomers based on pyrrole and thiophene: A versatile route to conducting block and graft polymers," Polym. Int. **52**, 1573–1578 (2003).

Yang, Y., Ding, S., Araki, T., Jiu, J., Sugahara, T., Wang, J., Vanfleteren, J., Sekitani, T., Suganuma, K., and Berlin, S.-V., "Facile fabrication of stretchable Ag nanowire/polyurethane electrodes using high intensity pulsed light," Nano Res. **9**, 401–414 (2016).

Yao, B., Wang, H., Zhou, Q., Wu, M., Zhang, M., Li, C., and Shi, G., "Ultrahigh-conductivity polymer hydrogels with arbitrary structures," Adv. Mater. **29**, 1700974 (2017).

Yuxin, L., Liu, J., Chen, S., Lei, T., Kim, Y., Niu, S., Wang, H., Wang, X., Foudeh, A. M., Tok, J. B.-H., and Bao, Z., "Soft and elastic hydrogel-based microelectronics for localized low-voltage neuromodulation," Nat. Biomed. Eng. **3**, 58–68 (2018).